Generalization of the Gouy-Chapman-Stern model of an electric double layer for a morphologically complex electrode: Deterministic and stochastic morphologies

Rama Kant* and Maibam Birla Singh
Department of Chemistry, University of Delhi, Delhi 110007, India
(Received 6 December 2012; revised manuscript received 21 September 2013; published 7 November 2013)

We generalize the linearized Gouy-Chapman-Stern theory of an electric double layer for morphologically complex and disordered electrodes. An equation for capacitance is obtained using a linear Gouy-Chapman or Debye-Hückel equation for the potential near the complex-geometry electrode-electrolyte interface. The effect of the surface morphology of an electrode on an electric double layer is obtained using multiple scattering formalism in surface curvature. The result for capacitance is expressed in terms of the ratio of Gouy screening length to the local principal radii of curvatures of the surface. We also include a contribution of a compact layer, which is significant in the overall prediction of capacitance. Our general results are analyzed in detail for two special morphologies of electrodes, i.e., a nanoporous membrane and a forest of nanopillars. Variations of local shapes and global size variations due to residual randomness in morphology are accounted for as curvature fluctuations over a reference shape element. In particular, the theory shows that the presence of geometrical fluctuations in porous systems causes an enhanced dependence of capacitance on mean pore sizes and suppresses the magnitude of capacitance. This theory is further extended to include contributions to capacitance from adsorption of ions and electrode material due to electronic screening. Our predictions are in reasonable agreement with recent experimental measurements on supercapacitive microporous and mesoporous systems.

DOI: 10.1103/PhysRevE.88.052303 PACS number(s): 82.45.Yz, 47.27.eb

I. INTRODUCTION

The electrochemical study of curved nanostructured surfaces (CNSs) is due to the need to develop efficient energy generating and storage devices [1] and electromechanical systems [2] as well as their applications in nanofluidics [3]. Recently, the electrochemical supercapacitive behavior of porous carbon materials [4], e.g., carbide derived carbons (CDCs) [1,5], activated carbons (ACs), graphitic carbon, and carbon nanotubes [2], has attracted intense focus. These supercapacitive systems, mainly based on the electrical double layer (EDL), require surfaces with high specific area and volume with proper pore size and shape control for the efficient access of ions to obtain high-energy storage as well as high power. Hence the EDL formed at the complex nanostructured or disordered interface is a major focus of research [3,4,6–13].

It is well known that electrochemical capacitance is strongly influenced by the morphology of nano- and mesoporous electrode materials [14]. Gogotsi and co-worker were successful in developing a supercapacitor with well controlled pore sizes in porous CDC material [1,5,15], which shows an anomalous behavior in the capacitance [16]. These experimental results show three regimes in the capacitance vs pore size data [1,5,15]: (i) a nonlinear increase in capacitance, (ii) the transition from micropore to mesopore capacitance with a minimum, and (iii) the anomalous increase and a maximum in capacitance of pores below 1 nm. Huang and co-workers [17–19] proposed a heuristic model for the capacitance of such a problem with an assumption of cylindrical pores. They included the effect of finite pore sizes and proposed three models for three different pore size regimes: (i) in the micropore regime (<2nm), the electric wire in cylinder capacitor model [18]; (ii) in the mesopores regime (2–50 nm), the electric double cylinder capacitor model [18]; and (iii) in the macropore regime (>50 nm) where curvature is no longer significant, the parallel plate capacitor model. A major advancement in the theory of porous electrodes has been achieved in recent years [10,20–22] that is applicable to supercapacitor and capacitive deionization or water desalination cells [23–25]. These works focused on the dynamics of ion transport in porous material, which is usually understood through the Nernst-Planck equation employing a generalized Furmkin-Butler-Volmer model boundary condition [20]. A classical Gouy-Chapman-Stern (GCS) model is proposed for macropores where the EDL is thin compared to pore size. In the case of micropores (where adsorption and overlapping of the EDL is important) a modified Donnan model is proposed [20–22] with the assumption that the potential inside the pore is constant. Two limiting regimes, the supercapacitor regime and the desalination regime [21,26], are identified in agreement with experiments [23]. However, these studies do not account for the detailed influence of the local shape, topology, and roughness. Computer simulations are becoming standard tools in studying EDLs on planar geometries [27–29], but recently have been applied to curved and porous systems [30–33], taking into account ion size, ion-ion correlation [28,29], and ion-solvent interaction [34,35]. Also simulations of EDLs have been done that take into account the dependence of the electrolyte dielectric permittivity on the local electric fields [36] in spheres and with electrodes made of closely packed monodisperse mesoporous spheres [37]. These simulations and theory do not account for the general geometrical features and morphological fluctuation in the electrode. Hence there is a need for a systematic rigorous theory to understand the capacitance of complex and disordered electrodes [38] that interpret capacitance behavior of such electrodes within the framework of electric double layer theories [9,10,20,21,39,40].

*rkant@chemistry.du.ac.in; http://people.du.ac.in/~rkant

The applied electrode material surfaces have ubiquitously complex morphologies. The modeling of such systems is difficult and complexity arises due to the pore structure with interconnected three-dimensional connectivity of pores of nonuniform shape and size. The morphology of the pores and particulate materials may be idealized to various forms: prolate, oblate, ellipsoidal, spheroidal, tubular, etc. These forms and morphologies can easily be identified by their local curvatures. The local surface shape at a point α on the surface is approximated as the deviation from a tangent plane as

$$z_\alpha = \tfrac{1}{2}[x^2 k_1(\alpha) + y^2 k_2(\alpha)], \tag{1}$$

where $k_1(\alpha) = 1/R_1$ and $k_2(\alpha) = 1/R_2$ are the curvatures at a point α and R_1 and R_2 are the principal radii of curvatures. Usually a surface may be characterized by two curvatures: mean and Gaussian. The mean curvature is the average of two principal curvatures [defined as $H_\alpha = 1/2(k_1 + k_2)$] and the Gaussian curvature is the product of the two principal radii of curvatures (defined as $K_\alpha = k_1 k_2$). Various shape configurations may be generated by varying the curvatures through k_1 and k_2. However, for a real pore the space will be a combination of these idealized shapes or can be looked upon as fluctuations in pore structure around one of these idealized shapes and hence identified with statistical properties of their curvatures.

In this article we develop a (linearized) Gouy-Chapman-Stern level theory for an arbitrary morphology. The theory is based on segregation of the compact layer and diffuse layer regions (see Fig. 1) with an assumption of the validity of the linearized Poisson-Boltzmann equation in the diffuse layer region while compact layer corrections are included at the level of local capacitance density. In Sec. II we explain the effect of the geometry and topology on the diffuse layer capacitance. In Sec. III we include the compact layer contribution to the diffuse layer capacitance on an arbitrary curved surface electrode. In Sec. IV we develop a theory for the nanostructured electrode with random morphology, viz., the curvature fluctuation in a porous system arises due to intrapore roughness and interpore size variations. General results are applied for a detailed analysis of the porous membrane and forest of nanorod electrodes. A comparison with recent experimental data of the capacitance to pore size is presented in Secs. V and VI. A summary is given and conclusions are discussed in Sec. VII.

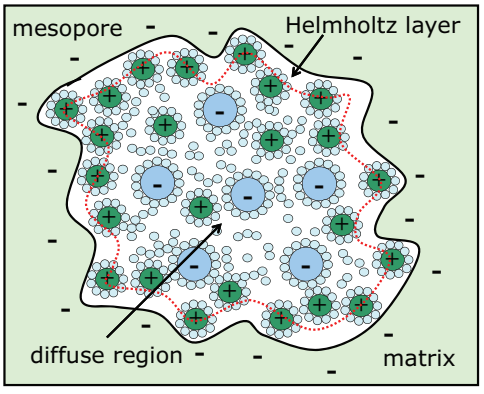

FIG. 1. (Color online) Schematic model of the EDL formed in an arbitrary nanoporous electrode showing the Helmholtz layer and the diffuse layer.

II. MODEL OF ELECTRIC DOUBLE LAYER NEAR CURVED SURFACES

The double layer is usually divided into two regions: the compact double layer (referred to as the Helmholtz double layer) comprised between the electrode and the surface of the closest approach and the diffuse double layer extending from the surface of the closest approach to the bulk of the solution. The overall potential drop ϕ_0 between the electrode and the bulk solution may be written as $\phi_0 = (\phi_{\text{surface}} - \phi_{\text{OHP}}) + (\phi_{\text{OHP}} - \phi_{\text{bulk}})$. Now differentiating the overall potential drop with the combined charge density σ (equal to the sum of the Helmholtz and the diffuse layer charges) at the interface we have

$$\begin{aligned} \frac{\partial \phi_0}{\partial \sigma} &= \frac{\partial(\phi_{\text{surface}} - \phi_{\text{OHP}})}{\partial \sigma} + \frac{\partial(\phi_{\text{OHP}} - \phi_{\text{bulk}})}{\partial \sigma}, \\ c_{\text{DL}}^{-1} &= c_H^{-1} + c_G^{-1}, \end{aligned} \tag{2}$$

where the term on the left-hand side of Eq. (2) is the inverse differential capacitance of the double layer c_{DL}. The first and second terms on the right-hand side of Eq. (2) are the inverse differential capacities of the compact Helmholtz layer c_H and the diffuse double layer c_G, respectively.

Historically, it was von Helmholtz [41], who first conceived of the idea that adsorption of opposite charge ions from solution on an electrode surface with an excess or deficiency of charge results in a situation like a parallel plate capacitor of opposite charge with a thickness of a few nanometers. The capacitance density of the Helmholtz layer (HL) [8] is

$$c_H = \frac{\epsilon_0 \epsilon_H}{r_H}, \tag{3}$$

where ϵ_0 is the dielectric constant of free space, ϵ_H is the HL relative dielectric constant, and r_H is the thickness up to the outer Helmholtz plane (OHP). Gouy [42] and Chapman [43] included the fact that the ions are mobile in the electrolyte solution due to thermal motion and developed a mathematical treatment based on the combined application of Boltzmann's energy distribution equation and Poisson's equation. However, the Gouy-Chapman model is known to overestimate the EDL capacitance for a planar electrode. The divergence was overcome by Stern [44] by combining in series both the HL capacitance c_H and the Gouy-Chapman capacitance of a planar electrode c_G as $c_{\text{DL}}^{-1} = c_H^{-1} + c_G^{-1}$, where $c_G = \epsilon \kappa_{\text{eff}}/4\pi$ and $\kappa_{\text{eff}} = \kappa \cosh(e\beta\phi_2/2)$, where $\phi_2 = (\phi_{\text{OHP}} - \phi_{\text{bulk}})$. The Debye-Hückel screening length $\kappa^{-1} = \ell_D = (\epsilon k_B T/4\pi e^2 \Sigma n_i^0 z_i^2)^{1/2}$, where T is temperature, k_B is the Boltzmann constant, ϵ is the dielectric constant of bulk electrolyte, n_i^0 is the number density of ith ion with charge $z_i e$, and e is the electronic charge. Nagy *et al.* showed that the dielectric constant in the HL capacitance ϵ_H should be the average of the inner layer and diffuse layer dielectric constants due to the polarization charges induced on the boundary of the Helmholtz and diffuse layers [27].

A general theory developed by Duplantier [45] for the free energy of the EDL of two interacting curved surfaces with a given orientation. This theory clearly shows that the interaction term has exponential decay $\exp(-\kappa d)$ with the shortest separation distance d in the unit of the Debye screening length κ^{-1}. Note that the free energy of the two interacting surfaces in

the electrolyte are related to the capacitance of these surfaces through the Lippmann equation [46]. Goldstein *et al*. drew a similar conclusion from the EDL near two modulated or rough surfaces [47]. The screened potential in the EDL decays exponentially with distance from a rough surface [47,48] and major deformation in equipotential surfaces near the electrode surface is limited up to a few Debye lengths, hence the shape and morphology of two well separated electrodes will influence their own contribution to the capacitance behavior. This implies that surfaces in electrolytes placed at a distance much larger than κ^{-1} (with nonoverlapping diffuse layers) act effectively as two independent surfaces and can be theoretically treated as two independent semi-infinite boundary value problems (where the bulk boundary condition is represented by a plane equipotential surface away from the arbitrary electrode surface).

The potential in the EDL can be obtained using the Poisson-Boltzmann equation (PBE). Tessier and Slater [49] have shown the validity of the PBE when the system size is reduced to nanoscopic and mesoscopic dimensions. The solution of Poisson's equation for the potential ϕ relative to the bulk electrolytes can be obtained under the condition of strong or weak potential approximations. Hence the simplifying assumption used in our work is that the region near an electrode is divided into two regions. One is a strong electric field region where a major change in electric potential occurs, i.e., the compact layer. This change continues in the region beyond the compact layer with a relatively weak electric field, i.e., the diffuse layer region (hence assumed to obey the linearized Gouy-Chapman equation or the Debye-Hückel equation). The linearized PBE for the potential $\phi(r)$ relative to the bulk solution is written as

$$(\nabla^2 - \kappa^2)\phi(r) = 0, \tag{4}$$

where the interfacial potential with respect to the bulk is taken as constant and the bulk electrolyte equipotential surface is a plane with the potential assumed to be zero. The solution of the Helmholtz equation or Debye-Hückel equation for arbitrary geometries and boundary conditions (Dirichlet, Neumann, or Robin) is known in the form of multiple scattering expansions [45,50–53]. Also the multiple scattering expansion in the curvature results accounting for the arbitrary geometry of the surface is analyzed for the diffusion problems [48,53–57]. Adapting a similar methodology to solve the electrostatic potential of the electric double layer, we will obtain the capacitance of the EDL near surfaces of arbitrary shapes in the Debye-Hückel or the linearized Gouy-Chapman regime.

Using Gauss's law, the local charge density σ_G in the diffuse electric double layer is $\sigma_G = (\epsilon/4\pi)(\partial\phi/\partial n)$, where ϕ is the potential relative to the bulk solution and $\partial/\partial n \equiv \hat{n}\cdot\nabla$ is the normal derivative (with unit normal vector $\hat{n}$ on the surface). Differentiating σ_G with respect to ϕ_2 gives the specific differential capacitance of a diffuse double layer $c_G = d\sigma_G/d\phi_2$ in terms of the electrostatic potential as

$$c_G = \frac{\epsilon}{4\pi}\frac{d}{d\phi_2}\left(\frac{\partial\phi}{\partial n}\right), \tag{5}$$

where ϵ is the dielectric constant of the bulk electrolyte and $\partial\phi/\partial n = \hat{n}\cdot\nabla\phi$ is the inward normal derivative of the potential to the surface at the OHP and is a functional of surface potential.

We use the method of the Green's function in order to obtain the various orders of the scattering terms depending on the surface curvature (detailed calculations are shown in Appendix A). The capacitance density at a point α of the surface in terms of the Green's function is obtained using Eq. (5) as

$$c_G(\alpha) = \frac{\epsilon\kappa^2}{4\pi}\int_V d^3r'\frac{\partial G(\alpha^+,r')}{\partial n_\alpha} = \frac{\epsilon\kappa^2}{4\pi}\int_V d^3r'\left[2\frac{\partial G_0(\alpha,r')}{\partial n_\alpha} - 2^2\int\frac{\partial G_0(\alpha,\beta)}{\partial n_\alpha}\frac{\partial G_0(\beta,r')}{\partial n_\beta}dS_\beta\right.$$
$$\left. + 2^3\int\frac{\partial G_0(\alpha,\beta)}{\partial n_\alpha}\frac{\partial G_0(\beta,\gamma)}{\partial n_\beta}\frac{\partial G_0(\gamma,r')}{\partial n_\gamma}dS_\beta dS_\gamma - \cdots\right], \tag{6}$$

where G is the Green's function (GF) and G_0 is the free space GF (other symbols are defined in Appendix A). The use of Eq. (1) for the local surface geometry approximation and the expansion of various terms in Eq. (6) for the convergence of the screening length power series are applicable in a strong screening regime, viz., the Debye-Hückel screening length κ^{-1} is smaller than any scale of the radius of curvature. Local and global curvatures in the geometric and topological features of the surface are expected to play a role in the formation of the electric double layer near a curved surface. The expansion is obtained in powers of κ^{-1}/R, where R is a typical radius of curvature. The convergence of the screening length power series is applicable in a strong screening regime, viz., the Debye-Hückel screening length κ^{-1} is smaller than any scale of the radius of curvature. The expansions will be obtained in powers of κ^{-1}/R, where R is a typical radius of curvature. The local shape of the interface is given by mean H_α and Gaussian curvatures K_α at the point α on the surface. Expressions of the various orders of the scattering terms are obtained in terms of two curvatures. The capacitance density of the diffuse layer is (see Appendix A for details)

$$c_G(H_\alpha,K_\alpha) = \frac{\epsilon\kappa}{4\pi}\left[1 - \frac{1}{\kappa}H_\alpha - \frac{1}{2\kappa^2}\left(H_\alpha^2 - K_\alpha\right) + \cdots\right]. \tag{7}$$

Equation (7) is retained up to second order in the curvature expansion where two curvatures satisfy $(H^2 - K) = 1/4\,(1/R_1 - 1/R_2)^2$ and $(H^2 - K) \geqslant 0$. Equation (7) clearly shows that the geometric dependence of the capacitance is controlled by the second and third terms through H and K. If $H = 0$ and $K = 0$, the diffuse layer capacitance simplifies to the flat surface (for small applied potential) Gouy-Chapman capacitance [58]. The local capacitance result for an arbitrary curved electrode has three terms. The first term is dependent on the solution properties, the second term is dependent on geometry (independent of ionic concentration), and the third term represents the coupling between geometrical and solution properties. As mention earlier, the EDL interface consist of two layers: a compact and a diffuse double layer. The diffuse double layer is separated from the electrode surface by the compact double layer. Thus we to have calculate the ionic capacitance with compact layer size corrections. In order to calculate the ionic capacitance of the diffuse layer in the curved geometry at the OHP, we have to account for the adjusted curvature due to the presence of a compact layer surface parallel to the original electrode surface. Since the compact layer surface is outside the electrode material (here, in solution), we consider the boundary of the compact layer surface to be at a distance of r_H in the normal direction from the electrode surface. The relation of the adjusted mean curvature H' and the adjusted Gaussian curvature K' on the parallel compact layer surface compared with the original electrode surface with mean and Gaussian curvatures H and K is given by [59]

$$H' = \frac{H - Kr_H}{1 - 2Hr_H + Kr_H^2}, \quad K' = \frac{K}{1 - 2Hr_H + Kr_H^2}, \tag{8}$$

where the local surface quantities $H = (1/R_1 + 1/R_2)/2$ and $K = 1/R_1R_2$ on the surface of electrode. For negligibly small r_H, we have $H' \approx H$ and $K' \approx K$. Substituting H' and K' into Eq. (7), we can obtained the ionic capacitance with compact layer size correction c_G.

We illustrate how to obtained the ionic capacitance using Eq. (7) in conjunction with Eq. (8) through its application to a cylindrical pore and a rod geometry. There are two curvatures for a cylindrical pore: The mean curvature $H = 1/2r$ is constant and the Gaussian curvature $K = 0$. Similarly, for a cylindrical rod, $H = -1/2r$ while $K = 0$. In Fig. 2 we show two cases of capacitance, viz., the linearized Gouy-Chapman (LGC) model capacitance for curved surfaces (dotted lines) and the LGC capacitance after Helmholtz layer size correction, which we call the adjusted LGC (AGC) capacitance for curved surfaces (solid lines); that is, for a cylindrical pore the adjusted curvature is $H' = 1/[2(r - r_H)]$ and for a cylindrical rod the adjusted curvature is $H' = -1/[2(r + r_H)]$. The diffuse layer capacitance given by Eq. (7) may be represented for simple curved surfaces as

$$c_G = c_0\left(1 + a\frac{l_D}{r_a} + b\frac{l_D^2}{r_a^2}\right), \tag{9}$$

where $c_0 = \epsilon_0\epsilon_D/l_D$ is the planar capacitance density and (a,b) are pairs of dimensionless numbers depending on the shape of a nanoelectrode, viz., (0,0) for a plane, $(-1/2,-1/8)$ for a cylindrical tube, $(1/2,-1/8)$ for a cylindrical rod, $(-1,0)$ for a spherical cavity, and (1,0) for a sphere. The effective adjusted radius is due to the compact layer ($r_a = r \pm r_H$) on

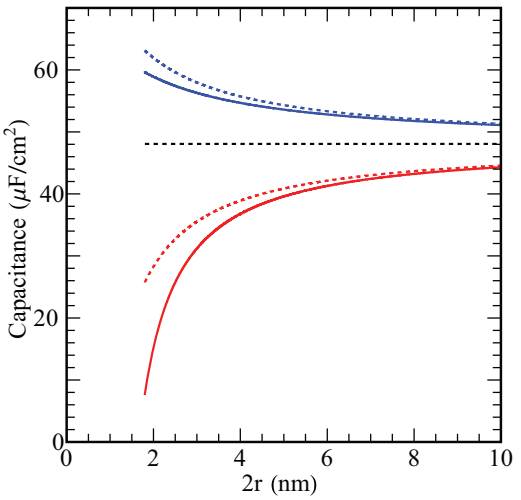

FIG. 2. (Color online) Theoretical capacitance density vs diameter plots for cylindrical pore and rod electrodes. The LGC capacitance curved surface (dotted lines) and adjusted LGC capacitance (solid lines) after inclusion of the Helmholtz layer size correction for pore (red line) and rod (blue line) geometries. The plots are generated using $r_H = 0.35$ nm, $\epsilon_H = 6$, and $\epsilon = 38$ for an organic electrolyte at 298 K.

curved surfaces, where the plus and minus signs are assigned to convex (e.g., a sphere or a cylindrical rod) and concave (e.g., a cylindrical tube or a spherical cavity) surfaces, respectively.

Figure 2 shows the plot for the capacitance of these simple geometries and their dependence on size $2r$. Here we show that the morphological influence of idealized geometries on capacitance is mainly due to the diffuse layer. The LGC and AGC capacitance curves for the pore have smaller values compared to the flat surface. In the case of a rod (red lines) we see that the LGC value increases with reduced rod diameter while for the AGC capacitance this increase weakens due to the larger adjusted rod diameter. This finding for the LGC capacitance is similar to Compton and co-workers' report of enhancement of capacitance in the diffuse layer for hemispherical and cylindrical electrodes [39,60]. However, with increasing sizes, all electrodes reach a curvature-independent capacitance value and merge with the planar capacitance limit. It is important to emphasize that our theory will be applicable to a porous system for pore sizes $2r > 2r_H + l_D$, i.e., sufficient to accommodate the compact as well as the diffuse layer inside them (the nonoverlapping EDL). An extension of the capacitance curves below the pore diameter $2r_H + l_D$ will require accounting for contributions from the Donnan contribution [20,21], the ion-ion correlation [10], and the material space charge [61,62].

Another important quantity of physical interest is the total diffuse layer capacitance of a nanostructured electrode C_D. This is obtained by integrating the local diffuse layer capacitance density c_G in Eq. (7) with respect to the interfacial surface as

$$C_G = \int dS\, c_G = \frac{\epsilon\kappa}{4\pi}\left[A - \frac{1}{\kappa}\bar{H} - \frac{1}{2\kappa^2}(\bar{H}^2 - \bar{K}) + \cdots\right]. \tag{10}$$

The morphological quantities $A = \int_S dS$ (geometric area), $\bar{H} = \int_S H dS$ (integral of mean curvature), and

$\bar{H}^2 = \int_S H^2 dS$ (integral of the square of mean curvature) and the topological quantity $\bar{K} = \int_S K\, dS$ (integral of Gaussian curvature) can be calculated for both regular and random geometries. Here K gives the intrinsic property and depends on how the distance is measured on the surface; H gives the extrinsic property and depends upon the local curvature at each point with no knowledge of the three-dimensional space in which it is embedded. The topological information for a surface is obtained through a Gauss-Bonnet theorem [63] as $\bar{K} = \int_S dS/R_1R_2 = 4\pi(N_c - N_h)$, where N_c is the number of connected surfaces (i.e., the number of membranes or electrodes) and N_h is the number of handles (genus or holes) for various topologies of individual membranes or electrodes on the surface. Here $N_h = 0$ for spheres, $N_h = 1$ for tori, etc. The electrode potential dependence from the above result (10) can be found in the observation of Daikhin *et al.* [64] that the result for the nonlinear Poisson-Boltzmann theory of capacitance at a rough electrode-electrolyte interface is related to the result for the linear version of the PBE. The effective nonlinear contribution of the PBE may be included in the linear solution by replacing the inverse Debye length κ with a potential-dependent inverse effective Debye or Gouy length $\kappa_{\text{eff}} = \kappa\, \cosh(e\phi_2/2k_BT)$ [58,65].

The capacitance of the EDL at the GCS level is usually obtained using an analogy of capacitors in series. Here we assume the validity of the ansatz of combining two components of capacitances in series as in Eq. (2). Two limiting situations for the local capacitance are observed due to different functional dependences of the charge on the electrolyte concentration and electrode potential. Two components of capacities are estimated in our analysis by dividing the region near an electrode into two regions. One is a strong electric field region where the capacitance is estimated using the Helmholtz formula. The region beyond the compact layer is the diffuse layer and has a relatively weak electric field. The diffuse layer capacitance is estimated through the AGC model for the curved interface. This approximation provides a workable simplicity to our model. Combining Eqs. (7), (8), and (2) we obtain the adjusted (linearized) Gouy-Chapman-Stern (AGCS) capacitance density for an arbitrary geometry electrode as a function of the mean and Gaussian curvatures:

$$c_{\text{DL}}(H,K) = \frac{c_H c_0\left[1 - H' l_D - (H'^2 - K')\left(l_D^2/2\right)\right]}{c_H + c_0\left[1 - H' l_D - (H'^2 - K')\left(l_D^2/2\right)\right]}, \tag{11}$$

where $c_0 = \epsilon\kappa/4\pi$ and $c_H = \epsilon_H\epsilon_0/r_H$, where ϵ_H is the electrolyte dielectric constant in the HL, ϵ_0 is the permittivity of the vacuum, and r_H is the effective thickness of the Helmholtz or compact layer. Here H' and K' are obtained at the Helmholtz surface [see Eq. (8)], respectively. The diffuse layer starts beyond the compact layer, hence the curvature adjusted at the Helmholtz layer is used in our calculation. The limiting case of planar EDL capacitance is obtained when $H' \to 0$ and $K' \to 0$. The effective or adjusted radii of curvatures at the diffuse layer are accounted for by subtracting r_H from or adding r_H to the radii of curvatures depending on the local convexity of the surface. Combining compact layer capacitance with AGC capacitance partially removes point particle limitations as well as the divergence under the $R/l_D \to 0$ limit. The local AGCS capacitance in Eq. (11) has three terms in the square brackets. The first term in square brackets is dependent on the solution properties, the second term is dependent on geometry through the local mean curvature, and the third term represents the coupling between geometrical and solution properties. The third term has mixed mean and Gaussian curvatures, viz., $H'^2 - K'$, which is equal to zero for spheres and hence measures the deviation from the local asphericity and follows the constraint $H'^2 - K' \geqslant 0$. Hence the local coupling between the geometry and ionic solution emerges due to deviation in the local asphericity of surface.

III. CAPACITANCE FOR RANDOM MORPHOLOGY ELECTRODES

Randomness arising due to disorder in porous material can be of three types: Pore roughness can be looked upon as (i) intrapore shape fluctuations along the contour of the pore, (ii) interpore size fluctuations over different pores, and (iii) fluctuations in the length of pores. The first two contributions of randomness can be accounted for through fluctuations in mean curvature. Some examples are as follows: CDCs have intrapore fluctuations, template carbon materials may have both intrapore fluctuations and interpore pore size fluctuations, and ACs and hierarchical porous graphitic carbon material [66] may have intrapore curvature fluctuations, pore size fluctuations, and pore length fluctuations. Fluctuations in the length of pores affect mostly the dynamic response of the pores [65,66]. This case is not required in calculations as one is not looking into the dynamical aspect of this problem.

The most appropriate method for characterizing the complex disordered structure is based on the statistical approach. Depending upon the nature of disorder in the nanostructured or porous electrode, one can have various distributions of curvature. We assume in our model an electrode with small random surface roughness around its reference geometry that is characterized in terms of an ensemble average mean and Gaussian curvatures, viz., $\langle H\rangle$ and $\langle K\rangle$. The surface roughness is characterized in terms of their deviations from the reference curvature, $H - \langle H\rangle$ and $K - \langle K\rangle$, with ensemble average mean values $\langle H - \langle H\rangle\rangle = 0$ and $\langle K - \langle K\rangle\rangle = 0$ but finite variance $\langle (H - \langle H\rangle)^2\rangle$ (a fourth-order term in the principle curvature, $\langle (K - \langle K\rangle)^2\rangle$, is assumed to be negligible). In order to calculate the capacitance of disordered systems, we take the statistical ensemble of various configurations in curvature space (for which the curvatures are distributed). Now the ensemble average capacitance density of the diffuse layer is obtained from Eq. (7) as

$$\langle c_G\rangle = c_0\left[1 - l_D\langle H\rangle - \frac{l_D^2}{2}(\langle H^2\rangle - \langle K\rangle) + \cdots\right], \tag{12}$$

where $\langle\cdot\rangle$ represent an ensemble average over all possible random surface configurations and $l_D = \kappa^{-1}$. Equation (12) has three terms: The first term is dependent on only the solution's ionic concentration, the second term is purely dependent on the ensemble average mean curvature, and the third term is due to coupling between the ionic solution and electrode morphology. The mean capacitance density $\langle c_G\rangle$ of the diffuse EDL will be strongly affected whenever the radii

of curvatures are comparable to the diffuse layer thickness, which is a strong function of electrolyte concentration.

The deviation in an ensemble average capacitance density is proportional to the difference of the curvature of the surface and the ensemble average curvature. The capacitance deviation of the diffuse layer $\delta c_G = c_G - \langle c_G \rangle$ is

$$\delta c_G = c_0\big[l_D(H - \langle H\rangle) - \big(l_D^2/2\big)(H^2 - \langle H^2\rangle) + \big(l_D^2/2\big)(K - \langle K\rangle)\big]. \tag{13}$$

The average deviation of capacitance is zero, i.e., $\langle \delta c_G \rangle = 0$. The mean square deviation of the difference of the capacitance density is obtained from Eq. (13) as

$$\big\langle \delta c_G^2 \big\rangle = c_0^2 l_D^2 \langle\!\langle (H - \langle H\rangle)^2 \rangle\!\rangle + O(H^4). \tag{14}$$

An important feature of practical surfaces is the presence of small surface roughness characterized as small fluctuations in surface curvatures about its reference geometry. We have truncated higher-order curvature contributions in Eq. (14). It is obvious from Eq. (14) that the ensemble average of the square of capacitance deviation is directly proportional to the ensemble average of the square of deviation in mean curvature. Rewriting Eq. (14) in terms of a coefficient of morphological fluctuations or relative variance of the mean curvature $\gamma^2 = \langle\!\langle (H - \langle H\rangle)^2 \rangle\!\rangle / \langle H\rangle^2$ we have

$$\big\langle \delta c_G^2 \big\rangle = \left(\frac{\epsilon}{4\pi}\right)^2 \gamma^2 \langle H\rangle^2 + O(H^4), \tag{15}$$

where γ is a coefficient of morphological fluctuations and is a measure of relative deviation from the mean curvature. This variance in capacitance density is independent of the concentration of electrolyte. The coefficient $\gamma < 1$ for weakly fluctuating interfaces and $\gamma \gg 1$ for strongly fluctuating interfaces.

As mentioned before, porous materials have complex spatial structures and are characterized by using morphological measures, viz., the mean (microscopic) geometric area of an electrode A, the ensemble average mean curvature $\langle H\rangle$, the ensemble average square of mean curvature $\langle H^2\rangle$, and the ensemble average of Gaussian curvature $\langle K\rangle$. For random ergodic fields [67] that are statistically homogeneous over various configurations, the (large) surface average over morphological quantities, viz., $\bar{H}/A$, $\bar{H}^2/A$, and $\bar{K}/A$ (as defined earlier), can be related to the ensemble average morphological quantities as $\langle H\rangle \equiv \lim_{A\to\infty} \bar{H}/A$, $\langle H^2\rangle \equiv \lim_{A\to\infty} \bar{H}^2/A$, and $\langle K\rangle \equiv \lim_{A\to\infty} \bar{K}/A$.

These morphological measures are in general useful in characterizing the structure of various materials, e.g., foams, gels, membranes, and granular and porous electrode systems. These measures can be calculated for both deterministic and stochastic geometries and are related through integral geometry to Minkowski functionals [68]. The ensemble average morphological measures now can be related through the above integral of mean curvature, the integral of mean square curvature, and the integral of Gaussian curvature. Hence, for a large nanostructured surface, Eqs. (10) and (12) are related through $\langle c_G\rangle \equiv \lim_{A\to\infty} C_G/A$. Since the reciprocal of compact and diffuse layer local capacitance is additive in nature we will perform averaging over an ensemble of random configurations. The ensemble average (inverse) capacity is now

$$\langle 1/c\rangle = \langle 1/c_H\rangle + \langle 1/c_G\rangle = 1/c_H + \langle\!\langle 1/(\langle c_G\rangle + \delta c_G)\rangle\!\rangle. \tag{16}$$

Using binomial expansion of the relative deviation in capacity, it simplifies to

$$\langle 1/c\rangle = 1/c_H + 1/\langle c_G\rangle + \big\langle \delta c_G^2\big\rangle / \langle c_G\rangle^3 + O\big(\big\langle \delta c_G^4\big\rangle\big). \tag{17}$$

Equation (17) for the random morphology electrode can be written as the ensemble average of the inverse of capacitance as

$$c_{\mathrm{DL}} = \left\langle \frac{1}{c}\right\rangle^{-1} = \left(\frac{1}{\langle c_S\rangle} + \frac{\beta^2}{\langle c_G\rangle}\right)^{-1}, \tag{18}$$

where $1/\langle c_S\rangle = 1/c_H + 1/\langle c_G\rangle$ and $\langle c_S\rangle$ is the mean compact and diffuse layer capacitance density for average surface morphology. The relative mean square fluctuation in capacitance $\beta^2 = \langle \delta c_G^2\rangle / \langle c_G\rangle^2$ is

$$\beta^2 = \frac{\gamma^2 l_D^2 (\bar{H}/A)^2}{\big\{1 - (\bar{H}/A) l_D - [(\bar{H}^2/A) - (\bar{K}/A)]\big(l_D^2/2\big)\big\}^2}, \tag{19}$$

where γ represent the extent of fluctuations in surface morphology.

Using an assumption of ergodic field [67], Eq. (18) in combination with Eqs. (12) and (15) simplifies to the mean EDL capacitance in two components. The nonfluctuating contribution $\langle c_S\rangle$ from this equation is represented as

$$\langle c_S\rangle = (1/c_H + 1/\langle c_G\rangle)^{-1} = \frac{c_H c_0\big\{1 - (\bar{H}/A) l_D - [(\bar{H}^2/A) - (\bar{K}/A)]\big(l_D^2/2\big)\big\}}{c_H + c_0\big\{1 - (\bar{H}/A) l_D - [(\bar{H}^2/A) - (\bar{K}/A)]\big(l_D^2/2\big)\big\}}. \tag{20}$$

The contribution from the fluctuating component $\beta^2/\langle c_G\rangle$ in the capacitance that arises due to the stochastic nature of the morphology is

$$\frac{\beta^2}{\langle c_G\rangle} = \frac{1}{c_0} \frac{\gamma^2 l_D^2 (\bar{H}/A)^2}{\big\{1 - (\bar{H}/A) l_D - [(\bar{H}^2/A) - (\bar{K}/A)]\big(l_D^2/2\big)\big\}^3}. \tag{21}$$

Equation (18) in combination with Eqs. (20) and (21) is the generalized average capacitance density c_d for an arbitrary random geometry. This expression relates the capacitance to the surface to the average mean and Gaussian curvatures of the random morphology electrodes. Hence the capacitance density c_d of the complex morphology electrode is dependent on an overall surface morphological and topological characteristics, viz., $\bar{H}$, $\bar{H}^2$, and $\bar{K}$.

A. Porous membrane with fluctuating pore sizes

The complex nature of the nanoporous electrode [20,21] may result in various distributions of surface shapes (curvatures) and pore lengths. In this section we model the influence of intrapore and interpore size fluctuations. Interpore size fluctuations arise due to the presence of polydispersity in pore sizes, which is often much larger than for intrapore fluctuations. Hence the nature of pore size and shape fluctuations is

critical in determining the capacitance of porous electrodes. For narrowly distributed pore sizes, e.g., CDC micropores with a mean pore size less than 2 nm, only the intrapore local surface fluctuations are significant. Low intrapore fluctuations are possible without choking the pore in the electrode. For broadly distributed mesopores not only is the fluctuation in interpore sizes important, but also the intrapore curvature fluctuations; hence there could be simultaneous contributions from both. The porous materials have pores of various sizes and shapes, e.g., activated carbons; such systems are approximated as membrane electrodes with micropores and mesopores.

Here we confine our analysis to the simple case of nanoporous materials as a porous membrane model that has an array of cylindrical pores. These pores are allowed to fluctuate weakly, so the topology of the membrane electrode is not changed. Typical geometrical features of the membrane are characterized by pore separation distance w, membrane thickness (pore length l), the outer macroscopic geometric area of the membrane electrode $2A_0$, and the number of pores N_h. In order to calculate N_h, we assume a simple model of the membrane with a hexagonal array of cylindrical pores whose number of pores is given by $N_h = 2A_0/[\sqrt{3}(2r + w)^2]$ [69], where r is the radius of the cylindrical pore. Since the number of pores per unit area is usually very large, on the order of 10^{12}, the area of two planar surfaces $2(A_0 - \pi r^2 N_h)$ connecting two ends of the pores of the membrane is small and hence can be neglected. The major part of the area contribution comes from the area inside the pores. The total internal area of such a porous surface is given by the area of the individual pore times the number of pores in the membrane electrode, which is $A \approx 2\pi r l N_h$. For a cylindrical pore, the mean curvature $H = 1/2r$ is constant and the average mean curvature is $\bar{H}/A = \int H dS/A = 1/2r$. Similarly, the square of mean curvature is $H^2 = 1/4r^2$ and the average square of mean curvature is $\bar{H^2}/A = \int H^2 dS/A = 1/4r^2$. The average Gaussian curvature of a porous membrane is calculated using the Gauss-Bonnet theorem as $\bar{K}/A = \int K dS/A = 4\pi(N_c - N_h)$, where N_c is the number of connected surfaces. For a single membrane electrode, the connected component $N_c = 1$ and $\bar{K}/A = (2/rl)(1 - N_h)/N_h \approx -2/rl$ (for the large N_h electrode).

Knowledge of various morphological measures for a given model allows us to illustrate the use of Eq. (18) or (20) under the smooth surface limit $\gamma \to 0$, hence taking the ion with the effective ion size in the HL or thickness of the HL r_H, and the diffuse layer of the EDL is assumed to start after the Helmholtz layer. The effective or adjusted pore radii for the diffuse layer are accounted for by subtracting the HL thickness r_H from the pore radius r, i.e., $r - r_H$. Substituting the morphological quantities in Eq. (20), an explicit equation for the smooth pore membrane is obtained as

$$\langle c_S \rangle_P = \frac{c_H c_0 \left[1 - l_D/2(r - r_H) - l_D^2/8(r - r_H)^2 - l_D^2/l(r - r_H) + l_D^2/N_h l(r - r_H)\right]}{c_H + c_0 \left[1 - l_D/2(r - r_H) - l_D^2/8(r - r_H)^2 - l_D^2/l(r - r_H) + l_D^2/N_h l(r - r_H)\right]}. \tag{22}$$

Similarly, the relative mean square fluctuation in capacitance β^2 due to curvature fluctuations in pore sizes or roughness along the contour of pores is

$$\frac{\beta^2}{\langle c_G \rangle} = \frac{1}{c_0} \frac{\gamma^2 \, l_D^2/4(r - r_H)^2}{\left[1 - l_D/2(r - r_H) - l_D^2/8(r - r_H)^2 - l_D^2/l(r - r_H) + l_D^2/N_h l(r - r_H)\right]^3}. \tag{23}$$

It may be noted from Eqs. (22) and (23) that for two components of the capacitance the density equation for mesopores and macropores $c_{\mathrm{DL}} = (1/\langle c_S \rangle_P + \beta^2/\langle c_G \rangle)^{-1}$ has a contribution from the Helmholtz layer, the diffuse layer, and morphological parameters, viz., the pore radius r, pore length l, number of pores N_h, and coefficient of fluctuation γ. The capacitance of porous surfaces has the form of a rational polynomial, viz., the Padé approximant [70], in the inverse adjusted pore size $r - r_H$. Equation (22) shows that the ionic concentration-dependent Debye length l_D and adjusted pore size $r - r_H$ are length scales that affect the capacitance of the porous membrane. Our model, in comparison to that proposed in Refs. [20,21], explicitly accounts for the morphological details of nanostructured electrodes and geometrical fluctuation in them, though the simplicity of the model is preserved using the Debye-Hückel assumption. However, in the simultaneous presence of micropores along with mesopores and macropores, an additional adsorption contribution needs to be accounted for from the modified Donnan model [20,21] to capacitance (e.g., in porous activated carbon electrode). As mentioned earlier, the diffuse layer contributions in Eqs. (22) and (23) have a solution property-dependent term, a geometry-dependent term, and a coupling term between the solution and geometry. For adjusted pore size $r - r_H = 1$ nm, the relative importance of these three terms for $l_D \approx 1$ nm (for $0.1M$ electrolyte solution) is $1, \frac{1}{2}, \frac{1}{8}$.

In Figs. 3(a) and 3(b) we analyze the effect of the Helmholtz layer thickness and the effect of the change of concentration (or Gouy length) in the absence of the fluctuations in the contour of the pore ($\gamma \to 0$), respectively. Figure 3(a) shows the AGCS capacitance density plots for the porous membrane electrode, but without pore diameter fluctuations ($\gamma = 0$). The curves show the effect of HL thickness on overall capacitance. These plots are obtained using Eq. (22) and show two regions of capacitance behavior (the macropore limit where capacitance is constant and the mesopore where the capacitance decreases with a decrease of pore size) and a crossover between them. The point particle nature of ions in a diffuse layer allows

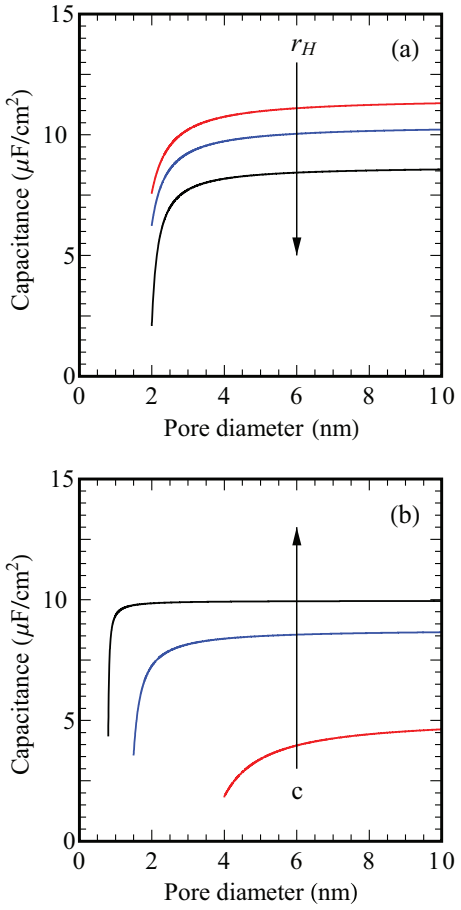

FIG. 3. (Color online) Capacitance plots for a porous membrane electrode with cylindrical pores obtained from Eq. (22) for a 1:1 organic electrolyte with $\epsilon = 38$ at 298 K. (a) Effect of compact layer thickness r_H on the capacitance profile. The plots are generated using concentration $c = 1M$, $\epsilon_H = 6$, and $r_H = 0.35$, 0.4, and 0.5 nm. (b) Effect of concentration on capacitance. The plots are generated using $r_H = 0.35$ nm and $\epsilon_H = 6$, while the concentrations used in various curves are $0.01M$, $0.1M$, and $1M$.

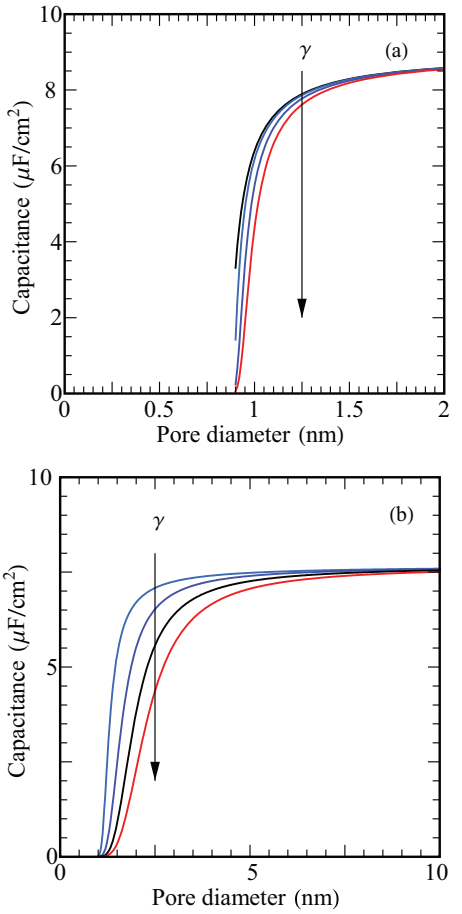

FIG. 4. (Color online) Effect of the morphological fluctuations in a porous membrane system on capacitance vs mean pore size plots. (a) Small fluctuation in pores sizes with $\gamma = 0$, 0.3, 0.6, and 0.9. (b) Large fluctuation in pores sizes with $\gamma = 2$, 4, 6, and 8. All plots are generated using $r_H = 0.35$ nm and $\epsilon_H = 6$ for a 1:1 organic electrolyte with $\epsilon = 38$ at 298 K.

us to extrapolate our capacitance vs pore size plot in the narrow pore size regime; however, this continuum model for the electrical double layer capacitance is valid up to a pore size with a cutoff $2r_H + \ell_D$, hence a prediction below this value (micropore) will require a dominant Donnan contribution (including adsorption) [20,21] from the electronic capacitance of the electrode [61,71,72]. These observations have been indicated in several experiments, but not captured by heuristic models [1,15,18]. The capacitance becomes independent of the pore size beyond 2 nm, while the experiments show a dependence up to 10 nm. This could be due to the exclusion of roughness or morphological fluctuations in porous electrodes.

Figure 3(b) shows the effect of concentration and pore size on the GCS capacitance density. Three curves are obtained for different concentration of electrolytes (or l_D). The conclusions that can be drawn from these curves are that for high concentration results $\kappa r > 1$ the pore size cutoff $2r = 2r_H + \kappa^{-1}$ decreases to a smaller pore size and the model is applicable to lower pore sizes and for low concentration results $\kappa r < 1$ there is a simultaneous increase in pore size cutoff value and gradual reduction of capacitance density. An anomalous increase in capacitance is observed in CDC where pore size is less than 1 nm [15], but this cannot be explained purely on the basis of ionic capacitance. The experimental capacitance density in Refs. [1,15,18] has a sudden rising region followed by a gently rising with increasing pore size and a crossover between these two regions. This is an interesting finding for a system with unimodal pore size, however, this is not seen in Figs. 3(a) and 3(b) as no influence of the fluctuation in pore sizes is included. The influence of fluctuation in capacitance behavior will be shown in Fig. 4.

In order to see the effect of morphological fluctuation on capacitance density, we plot the capacitance of a porous membrane electrode. The pore shape and size can fluctuate along the contour of the pore. Figure 4 shows the effect of surface morphological fluctuations on the capacitance of a porous membrane electrode. Figure 4(a) describes the capacitance vs mean pore size in the presence of small fluctuations in the micropore regime. We observe from the curves that as we increase the value of the surface morphological fluctuation parameter γ, the sudden rise region becomes weaker while the slow rise region develops a slightly faster rise. All the

curves merge around 2 nm and no effect of small fluctuations is seen beyond this. Thus the small fluctuations in micropores are important up to 2 nm. Figure 4(b) shows the effect on capacitance due to large fluctuations in the mesopore regime. As we increase γ, the value of capacitance is lowered compared to the smooth porous electrode. The effect of large fluctuations is seen for pore diameters much larger than $2r_H + l_D$. Increasing the mean pore size in the mesopore regime reduces the influence of fluctuation and finally all the curves merge around 10 nm. No curvature effect is seen beyond 10 nm, which suggests that large morphological fluctuations enhance the capacitance dependence on mean pore size up to 10 nm. This is in agreement with several experimental reports of capacitance vs pore size data (see the comparison with experimental data). The small fluctuation ($\gamma < 2$) affects the micropore regime while large fluctuations ($\gamma > 2$) affect the capacitance in the mesopore regime. For pore diameter less than 2 nm, the slope of the rapid rise region is almost the same. In the case of mesopores the fluctuation results in a decrease of capacitance. The larger the fluctuation is, the larger the pore size up to which the effect is seen. The capacitance increases rapidly in the transition region between micropores and mesopores followed by a gradual increase in the mesoporous regime and a limiting plateau value of a flat electrode is observed at large mesopores. Hence large morphological fluctuations play an important role in the enhancement of the capacitance density dependence on mean pore size.

B. Forest of nanorods with morphological fluctuations

In this section we obtain the capacitance for the forest of nanorods and compare it to that of nanopores. These two systems differ only in the convexity of their electrode surface. Such geometries are often employed in Li-ion batteries [73] and Al nanowire supercapacitors [74]. The typical dimension of the forest of nanorod electrodes is characterized by rod separation distance w, electrode thickness (rod length l), geometric area A_0, and number of rods N_r. In order to calculate N_r we assume an electrode with a hexagonal array of cylindrical rods whose number of rods is given by $N_r = 2A_0/[\sqrt{3}(2r + w)^2]$, where r is the radius of the cylindrical rod. The total area of such a structured surface of a forest of nanorods is given by the area of an individual rod times the rod density N_r, which is $A \approx 2\pi r l\ N_r$. Our theory is applied to the nanoforest electrode with inter-rod separation w, which can accommodate a compact as well as a diffuse layer between them, viz., $w \gg 2r_H + l_D$. The capacitance for an array of cylindrical rods is obtained by replacing $\bar{H}/A = (-1/2r)$ and $\bar{H}^2/A = (-1/2r)^2$ and the adjusted rod size for the diffuse layer is obtained by adding the compact layer thickness to the rod radius: $r + r_H$. Here the diffuse layer starts after a distance $r + r_H$ from the center of each rod. The average Gaussian curvature of the nanorods forest is calculated using the Gauss-Bonnet theorem as $\bar{K}/A = \int K\, dS/A = 4\pi(N_c - N_h)/A$. Using Eq. (20) we obtain the mean capacitance for N_r electrically connected forests of nanorods, with $N_c = N_r$, $N_h = 0$, and $\bar{K}/A = (2/rl)$:

$$\langle c_S\rangle_R = \frac{c_H c_0\left[1 + l_D/2(r + r_H) - l_D^2/8(r + r_H)^2 + l_D^2/l(r + r_H)\right]}{c_H + c_0\left[1 + l_D/2(r + r_H) - l_D^2/8(r + r_H)^2 + l_D^2/l(r + r_H)\right]}. \tag{24}$$

The relative mean square fluctuation in capacitance that arises due to surface fluctuations over rods is obtained using Eq. (21) as

$$\frac{\beta^2}{\langle c_G\rangle} = \frac{1}{c_0}\frac{\gamma^2 l_D^2/4(r + r_H)^2}{\left[1 + l_D/2(r + r_H) - l_D^2/8(r + r_H)^2 + l_D^2/l(r + r_H)\right]^3}. \tag{25}$$

Figure 5(a) shows plots of the effect of HL thickness on the GCS capacitance density vs rod diameter in a forest of nanorod electrodes where $\gamma = 0$. The plots are made using Eq. (24). As we increase the HL thickness, the value of capacitance decreases. The HL increases the adjusted radii of curvature of rods, resulting in a decrease in capacitance contributions from the diffuse layer. Figure 5(b) shows the effect of diffuse layer thickness, which increases with a decrease in the concentration of electrolyte, leading to a decrease in capacitance. Thus, for nanorods with the larger adjusted radii of curvature, the effect will largely be seen in the capacitance for the dilute solution. In the case of a concentrated solution, it simply increases the capacitance, but no enhancement in capacitance is seen in microrods.

Figure 5(b) shows the effect of concentration on the capacitance of an assembly of nanorod electrodes using Eq. (24) (the $\gamma = 0$ case). Unlike the cylindrical pore geometry, the capacitance of rod geometry is enhanced with a reduction in diameter. The overall capacitance is very much like the Helmholtz capacitance, but it is enhanced mainly for small rod diameter. An increase in concentration results in higher capacitance. We compare the capacitance obtained in the porous membrane electrode with nanorods with the same surface area, but different (local) convexity can have a qualitatively different capacitance dependence on size. These are purely geometric effects of the surface curvatures. Thus it can be concluded that membrane electrodes with cylindrical nanopores have different capacitance as compared to the forest of cylindrical nanorods, although both have the same geometrical surface area. We see from the plots that the curvature strongly affects the diffuse layer capacitance. Similar studies by Compton and co-workers [39,60] have shown that for hemispherical and nanotube electrodes, there is enhanced diffuse double layer capacitance due to an increase in curvature. In fact, our

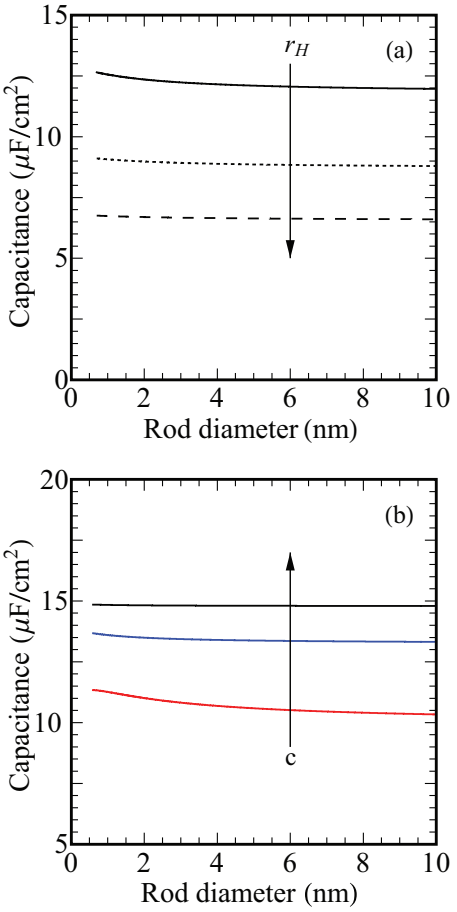

FIG. 5. (Color online) Capacitance plots for an assembly of cylindrical rods with no morphological fluctuation ($\gamma = 0$) obtained from Eq. (22). (a) Influence of the compact layer thickness r_H, e.g., 0.34, 0.4, and 0.7 nm. (b) Influence of the electrolyte molar concentration, e.g., $0.01M$, $0.1M$, and $1M$. All the plots are generated using $r_H = 0.34$ nm. Here $\epsilon_H = 6$ for a 1:1 organic electrolyte with $\epsilon = 38$ at 298 K.

analytical model calculations also show such an increase in diffuse double layer capacitance. However, the introduction of the compact (Helmholtz) layer capacitance in series with the diffuse layer capacitance reduces the total capacitance. Here the overall capacitance is controlled by the smaller of the two. It is important to note that the curvature effect is very much reduced in the case of nanorod electrodes, unlike the diffuse layer capacitance without adjusted radius correction. Furthermore, as we decrease the concentration and hence increase the Debye length, we see the curvature effect on capacitance reduced. The diffuse layer is extended in the low concentration regime and may require accounting for overlapping of the EDL [75,76].

Figure 6 shows the effect of morphological fluctuations on the capacitance of the forest of nanorods. By increasing the curvature fluctuation parameter γ, the capacitance behavior of the nanorods changes qualitatively from smooth nanorod capacitance behavior to nanoporous capacitance behavior. For $\gamma = 2$, the curve approaches nearly a horizontal line of a planar electrode and effectively no curvature effects are seen. The curves show a decrease in capacitance with an increase in

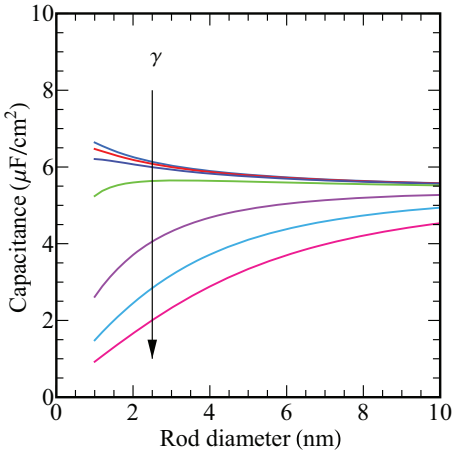

FIG. 6. (Color online) Effect of morphological fluctuations on the capacitance of a nanorod forest electrode. Here the fluctuation parameter is varied as $\gamma = 0.3$, 0.6, 0.9, 2, 4, 6, and 8. All the plots are generated using $r_H = 0.25$ nm and $\epsilon = 6$ for $0.05M$ H_2SO_4 with $\epsilon = 78.6$ at 298 K.

the value of γ and the curves appear similar to porous electrode capacitance with a gradual fall in smaller rod thickness. The physical reason is that for an assembly of nanorod electrodes with large curvature fluctuations on the nanorods result in the formation of pits or a porelike structure, which makes the capacitive response behave like a porous system.

IV. VOLUMETRIC CAPACITANCE OF THE NANOPOROUS MEMBRANE AND NANOFOREST OF RODS

Figure 7 shows the volumetric capacitance of a nanoporous membrane and a nanoforest of rods without morphological fluctuations. The expression of volumetric capacitance may be obtained by multiplying the area specific capacitance given by Eqs. (20), (22), and (24) with a surface area

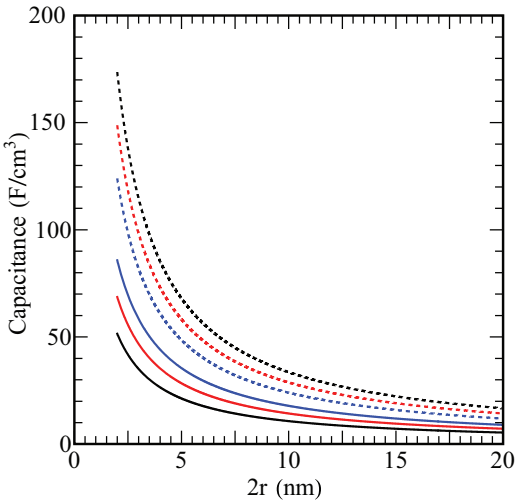

FIG. 7. (Color online) Volumetric capacitance of the nanoporous membrane and nanoforest of rods with different porosity Φ. The black, red, and blue lines correspond to $\Phi = 0.3$, 0.4, and 0.5, respectively. All the plots are generated using $r_H = 0.34$ nm. Here $\epsilon_H = 6$, $\epsilon = 38$, $l = 15$ nm, and $l_D = 0.7$ nm.

to macroscopic volume ratio. The detailed expression of volumetric capacitance of a nanoporous membrane and a forest of nanorods is given in Appendix B. Figure 7 shows the dominance of a specific area effect over the geometric effect emphasized in earlier plots (see Figs. 2, 3, and 5) of the capacitance. The solid and dashed lines correspond to the volumetric capacitance of a nanoporous membrane and a nanoforest of rods, respectively. The plots show clearly that the volumetric capacitance of a nanoforest of rods is larger than the volumetric capacitance of nanoporous membranes with the same volume. However, both geometries show the same trend of increasing capacitance for smaller pore or rod size due to increasing area for fixed porosity. We conclude that the area effect dominates the shape effect of the electrode when we consider the volumetric capacitance. It is found that increasing the porosity in the nanoporous membrane enhances the volumetric capacitance, while in the case of a forest of nanorods it suppresses the volumetric capacitance.

V. COMPARISON OF THEORETICAL RESULTS WITH EXPERIMENTAL DATA

Figure 8 shows the theoretical and experimental capacitance behavior of the organic electrolyte tetraethylammonium tetrafluoroborate ($TEABF_4$) in CH_3CN in different pore size regimes and concentrations. Data were taken from Refs. [1,15,18]. The dielectric constant of the solvent CH_3CN is taken to be 38 [8] at 298 K. The bare ion diameters of TEA^+ and BF_4^- are 0.68 and 0.46 nm, respectively [77]. We use in our calculations for the compact layer dielectric constant $\epsilon_H = 5.3$ [8] and the bare ion radius of TEA^+ is used as the compact layer thickness $r_H = 0.34$ nm. The plots are obtained

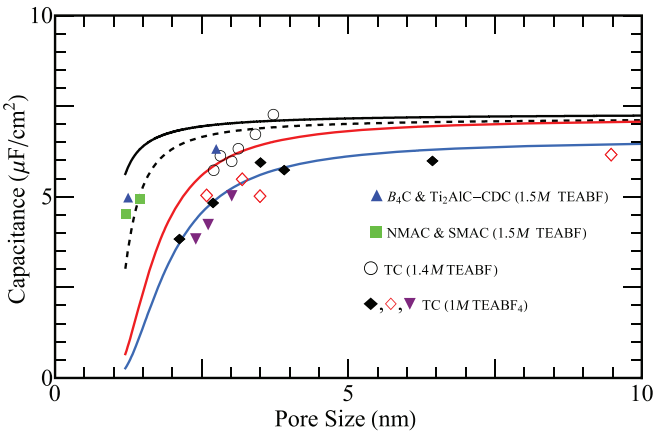

FIG. 8. (Color online) Theoretical capacitance curves for a porous membrane electrode model of the electrode with and without morphological disorder. Experimental data points are from Refs. [1,15,18] for various nanocarbons obtained by different methods with different morphology. The solid black line is for $1.5M$ $TEABF_4$ organic electrolyte in acetonitrile with $\epsilon = 38$ at 298 K, $\epsilon_H = 5.3$, $r_H = 0.34$ nm, and $\gamma = 0$. The dashed black line is the same case as the solid but with $\gamma = 2$. The solid red line is for a $1.4M$ concentration and $\gamma = 6$, with the rest of the parameters the same. The solid blue line is for a $1M$ concentration and with the rest of the parameters the same. Here NMAC stands for natural material precursor activated carbon and SMAC for synthetic material precursor activated carbon.

using Eq. (20) for smooth pores and Eq. (18) in combination with Eqs. (22) and (23). The theoretical plots for capacitance clearly indicate a fall in capacitance for smaller pore electrodes in an organic electrolyte. The solid black line is for $1.5M$ electrolyte and electrode without morphological disorder, i.e., $\gamma = 0$. The dashed black line is for the same concentration of electrolyte but with small morphological fluctuations γ (=2), viz., the CDC electrode material has a narrow pore size distribution, hence we use small value of γ (=2) in the theoretical curves. Similarly, the two lower curves (solid red and blue lines) have the template carbon (TC) electrode material, but differ in electrolyte concentration. Since the TCs have a large pore size distribution morphological disorder parameter γ (=6) is used to fit the experimental capacitance data. Two electrolyte concentrations of $1.4M$ and $1M$ are compared with the experimental data to illustrate the point that capacitance is dependent on the electrolyte concentration. The $TEABF_4$ in CH_3CN at $1.4M$ has a higher capacitance than the $1M$ $TEABF_4$ in CH_3CN for porous electrodes with $\gamma = 6$. In agreement with the theoretical prediction, the effect of morphological fluctuation is seen up to 10 nm in the experimental data [see the data set for TC ($1M$ $TEABF_4$) in Fig. 8].

The experimental comparison can further improve with inclusion of the contributions from electronic space charge capacitance of the electrode materials [61,62,71] and adsorption as these contributions will be important in the understanding of the anomalous rise region and its maximum. This is discussed in the following section.

VI. ANOMALOUS CAPACITANCE IN MICROPORES: ADSORPTION AND ELECTRODE MATERIAL CONTRIBUTIONS

In recent experiments [1,15,16,78] an anomalous increase in the capacitance with a decrease of the pore size (less than 1 nm) and a peak (maximum) at a particular pore size is observed. This feature is observed in both organic electrolytes [78] and ionic liquids [16]. Several attempts have been made to explain the pore size dependence of the capacitance in micropores. The increase in capacitance with decreasing pore size is explained in terms of the ion desolvation mechanism in an organic electrolyte [78] and the electrostatic image energy contribution to the free energy of the transfer of ions [79,80]. An atomistic molecular dynamics simulation for an ionic liquid confined inside a idealized nanotube also showed the increase in capacitance as the diameter of the tube decreases with ion size [31,33] but underestimated the experimental capacitance value due to the neglect of the electronic screening contribution [33]. A similar study was recently made on disordered carbon nanopores [81] accounting for potential-dependent adsorption while providing a model of charge storage in nanoporous materials. For a mesoscopic pore size the classical density functional theory [82,83] and molecular dynamic simulation [84] predicted that the specific capacitance oscillates with the pore size and is similar to the mean spherical approximation model [85].

Another approach for estimating the adsorption contribution to capacitance in micropores is based on the equilibrium distribution of ions between micropores and macropores. This

approach is called the modified Donnan model and is based on the assumption of a constant electrostatic potential inside the micropore to allow estimation of the number of cations or anions in the micropore $n_{\rm mi}$ [20,21],

$$n_{\rm mi} = n_0 \exp\left(\frac{-z_i e\Delta\phi_D + \mu_{\rm att}}{k_B T}\right), \tag{26}$$

where n_0 is the bulk ion number density, z_i is the charge of ion, $\Delta\phi_D$ is the Donnan potential, and $\mu_{\rm att}$ is the attraction term of ions adsorbing in micropores in the absence of applied voltage [20,23,25,26]. This approach does not include the dependence of capacitance on the size of the micropore. The dependence of the size of the micropore on capacitance can be included by combining a modified Donnan model and an electric wire in cylinder capacitor (EWCC) model.

Here we assume that micropores are cylindrical and the inner pore space is almost filled by adsorbed ions forming a wire of ions. The volume of the wire is equal to the volume of ions adsorbed inside the pore, i.e., $\pi a^2 l_p = \frac{4}{3}\pi a_0^3 (n_{\rm mi}/n_p)$, where a is the effective radius of the wire of ions, a_0 is the radius of the bare ion, and l_p is the penetration length of the ion. The number of ions in a single pore is the ratio of the number concentration $n_{\rm mi}$ [given by Eq. (26)] and micropore density n_p. The micropore density is calculated using the model of a hexagonal array of cylindrical pores (see Sec. III A) and $n_p = N_h/A_0 l_p \approx 10^{18}$ cm^{-3} for $l_p = 10$ nm. Now the capacitance contribution due to ion adsorption can be written as an EWCC equation [17,18]

$$c_{\rm ad} = \frac{\epsilon\epsilon_0}{r\ln(r/a)}, \tag{27}$$

where ϵ is the dielectric constant in a micropore and r is the radius of a micropore. The effective radius of the inner cylindrical wire due to an adsorbed ion a is

$$a = \sqrt{\frac{4a_0^3 n_{\rm mi}}{3l_p n_p}} = \sqrt{\frac{4a_0^3 n_0}{3l_p n_p}} \exp\left(\frac{-z_i e\Delta\phi_D + \mu_{\rm att}}{2k_B T}\right), \tag{28}$$

where the last term is obtained by substituting the value of $n_{\rm mi}$ given by Eq. (26). The value of $n_{\rm mi}$ is obtained using the bulk ion density n_0 calculated from the dimension of ions of ionic liquid 1-ethyl-3-methylimidazolium bis(trifluoromethane-sulphonyl)imide (EMI TFSI). The EMI has a dimension of 0.43 nm [1,16] along the short dimension and 0.76 nm [1,16] along the long dimension and the volume of the ion (assuming it to be a cylindrical rod) is $V_{\rm ion} = 0.441$ nm^3. The effective radius of the spherically shaped ion is $r_V = (3V_{\rm ion}/4\pi)^{1/3} = 0.47$ nm. If effective spheres of radius r_V are closely packed in a cubic arrangement, the volume of the cube will be $8r_V^3$ and the molar concentration will be $(8N_A r_V^3)^{-1} \approx 1.7M$ [86] (where N_A is Avogadro's constant) (the corresponding number concentration of the ionic liquid is $n_0 \approx 10^{27}$ cm^{-3}). The dashed black line in Fig. 9 represent the size-dependent adsorption capacitance as a function of pore size. The plot is generated with the following parameters: $\epsilon = 1$ (vacuum value), $\mu_{\rm att} = 8.62$ mV ($\approx 3k_B T/e$) [20,21,23], $T = 333$ K [16], $\Delta\phi_D = 0.517$ V ($\approx 18k_B T/e$), and $a_0 = 0.38$ nm (half along the long dimension) [16,18].

The electrode material contribution to capacitance can be obtained from our recent model, where we have generalized

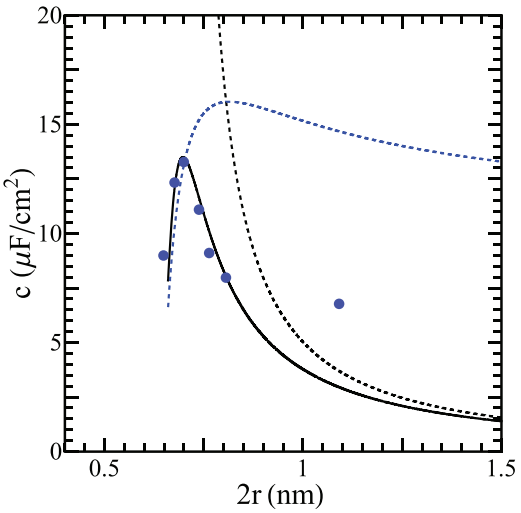

FIG. 9. (Color online) Theoretical capacitance with experimental data [1,16] for microporous CDC in ionic liquid EMI TFSI (blue circles).

the Thomas-Fermi electronic screening contribution for the capacitance of curved nanostructured electrodes [72]. This work shows shape-dependent localization and enhancement and reduction of capacitance in conducting and semiconducting nanomaterials. The electronic capacitance of cylindrical subnanopores is given by [72]

$$c_E = c_M\left(1 + \frac{l_{\rm TF}}{2(r-\delta)} - \frac{l_{\rm TF}^2}{8(r-\delta)^2}\right), \tag{29}$$

where $c_M = \epsilon_M\epsilon_0/l_{\rm TF}$ [87,88] is the planar electronic capacitance, r is the radius of the pore, δ is the electron spillover distance, and $l_{\rm TF} = \sqrt{\epsilon_0\epsilon_M/eD_0}$ is the electronic screening length. Here ϵ_M is the material dielectric, e is the electron charge, and D_0 is the density of state of the material. The dashed blue line in Fig. 9 represents the electronic capacitance of a cylindrical nanopore. The plot is generated using the following physical parameters: $\epsilon_M = 3.28$ (typically of graphite [61,62]), $D_0 = 2.46 \times 10^{21}$ cm^{-3} eV^{-1} (typical of metals as it is found that graphite behaves more like a metal in such cases [61,62,71,89]), and $\delta = l_{\rm TF} \approx 0.27$ nm (the diffuse character of the electron density and spillover contribute to the capacitance [33]). The electronic capacitance shows a maximum in capacitance with a rapid fall for smaller pore size and gradual fall for increasing pore size (see the dashed blue line in Fig. 9). This feature is similar to the experimental capacitance data of CDC (with pore size less than 1 nm) in ionic liquid. Our theory suggests that the electronic capacitance is responsible for the maximum and rapid fall in capacitance of the micropore. The experiment shows the maximum capacitance at smaller pore size than predicted by pure electronic capacitance theory, thus suggesting that the experimental value of capacitance is jointly given by the electronic and adsorption contributions.

In order to understand the overall behavior of capacitance with decreasing size of micropores, we combine the contribution from two factors, viz., the capacitance due ion adsorption given by Eq. (27) and the electronic capacitance given by

Eq. (29). The capacitance of micropore c can be written as

$$c^{-1} = c_E^{-1} + c_{\rm ad}^{-1}. \tag{30}$$

The solid black line in Fig. 9 shows a comparison of the theoretical capacitance of micropore c to the experimental data of CDC in the ionic liquid EMI TFSI. The plot is generated with the same parameters used in calculating $c_{\rm ad}$ and c_E. We observe that the theoretical capacitance c agrees well with the experimental data. It shows an anomalous (steep rise) capacitance for pore size less than 1 nm with the maximum capacitance corresponding to a pore size of 0.38 nm.

VII. CONCLUSION

In summary, a model for EDL capacitance in curved nanostructured and mesostructured electrodes was proposed within the framework of classical (linearized) Gouy-Chapman-Stern theory. Our analytical theory for electric double layer capacitance is applicable to a wider class of electrode morphology, topology, and electrolyte systems. A theory for an arbitrary electrode geometry was developed using the multiple scattering formalism of surface curvature. The capacitance in the diffuse layer is expressed through a convergent expansion in powers of the ratio of the Debye length to the principal radii of curvatures of the interface. The contribution of the compact layer and its size correction in the adjusted curvature for diffuse layers has a strong effect on the local capacitance. This was introduced through the capacitance in the series behavior of the local compact layer and local diffuse layer contributions. The theory was further extended for realistic electrodes with a ubiquitous morphological disorder or roughness that is characterized through a variance in mean curvatures. Our theory is general enough to handle the arbitrary morphology of an electrode, but we illustrated its significance for the simple system of a forest of cylindrical nanopillars and a nanoporous membrane with the added complexity of morphological disorder. The theory allowed us to analyze the effect of concentration, compact layer thickness, and shapes and their fluctuations for systems with a separation between two nanostructure elements or pore size larger than $2r_H + l_D$.

This paper further establishes for the capacitance of nanostructured electrodes the following points. The capacitance increases towards larger pore sizes with a limiting capacitance plateau (at planar) and concurs with experimental data. The capacitance for a nanoporous membrane electrode and a nanoforest electrode, with the same geometric area, highlights a qualitatively different effect of shape on the capacitance as a function of size. Hence the overall convexity of the electrode surface has a profound effect on the ionic capacitance. The curvature fluctuations in the electrode have a significant influence on the capacitance in the mesoscopic region. The small curvature fluctuations along the contour of pore or intrapore geometric fluctuations affect the increase of capacitance, which extends up to 2 nm. Hence weak intrapore fluctuations slightly enhance the pore size dependence of the capacitance. The effects of large curvature fluctuations manifest themselves through prolonged dependence of capacitance on pore sizes and persist in up to nearly 10 nm in the mesopore regime. Surprisingly, the large fluctuations in nanorod forest electrodes result in a qualitatively different dependence on rod thickness. We also show that the volumetric capacitance increases with decreasing pore or rod size. The volumetric capacitance of the nanoporous membrane is enhanced with porosity, whereas it decreases with porosity in the case of a nanoforest. This theory also accounts for quantum mechanical contributions from electronic space charge (i.e., generalized Thomas-Fermi quasiclassical theory for electronic screening capacitance) and ion adsorption (i.e., pore-size-dependent modified Donnan adsorption capacitance) in the micropores. Reasonable agreement with experimental data is shown in micropores.

Finally, our model is a step forward in the development of a general understanding of capacitance in complex interfacial systems. Analogous problems of finding the effect of nonideality of the electrode surface, compact layer disorder, and dynamic frequency-dependent response of nanostructured and porous electrodes are beyond the scope of the present paper.

ACKNOWLEDGMENTS

M.B.S. acknowledges support from UGC, New Delhi through a Research Fellowship in Science for Meritorious Students. R.K. is grateful to University of Delhi and DST for a grant (SERB research project SB/S1/PC-021/2013).

APPENDIX A

The Debye-Hückel or linearized Gouy-Chapman equation for the potential relative to the bulk solution $\phi(r)$ is

$$(\nabla^2 - \kappa^2)\phi(r) = 0 \tag{A1}$$

for a domain D bound by a conducting surface S (taken to be at the OHP), which is held at constant potential $\phi^+|_S = \phi_2$, and far away from this surface a equipotential plane surface, viz., $\phi(r \longrightarrow \infty) = 0$. The Green's function G for a linearized PBE (A1) satisfies

$$(\nabla^2 - \kappa^2)G(r,r') = -\delta^3(r - r') \tag{A2}$$

with the homogeneous boundary conditions at the surface S and far away from surface ($r \longrightarrow \infty$), viz., $G|_S = 0$. Actually G will be discontinuous at the surface and the boundary condition will be approached from the interior, i.e., $r' \to \beta^+$. The solution of Eq. (A2) for the potential relative to the bulk solution $\phi(r)$ can be formally written as [51]

$$\begin{aligned}\phi(r) &= \phi_2 \int_S dS_\beta \frac{\partial G(r,\beta^+)}{\partial n_\beta} = -\phi_2 \int_V d^3r' \nabla^2 G(r,r') \\ &= \phi_2 \left(1 - \kappa^2 \int_V d^3r' G(r,r')\right).\end{aligned} \tag{A3}$$

We seek to express G in terms of $G_0(r,r') = (1/4\pi|r - r'|)e^{-\kappa|r-r'|}$, the free space Green's function satisfying Eq. (A2) for the entire infinite domain. The Green's function G is expressed as [51]

$$\begin{aligned}G(r,r') = G_0(r,r') &- 2\int G_0(r,\alpha)\frac{\partial G_0(\alpha,r')}{\partial n_\alpha} dS_\alpha \\ &+ 2^2 \int G_0(r,\alpha)\frac{\partial G_0(\alpha,\beta)}{\partial n_\alpha}\frac{\partial G_0(\beta,r')}{\partial n_\beta} dS_\alpha dS_\beta \\ &+ \cdots .\end{aligned} \tag{A4}$$

Using Gauss's law and the fundamental singularity at the boundary [50,51], the differential capacitance density is

$$\begin{aligned} c(\alpha) &= \frac{\epsilon\kappa^2}{4\pi}\int_V d^3r' \frac{\partial G(\alpha^+,r')}{\partial n_\alpha} \\ &= \frac{\epsilon\kappa^2}{4\pi}\int_V d^3r' \Bigg[2\frac{\partial G_0(\alpha,r')}{\partial n_\alpha} \\ &\quad - 2^2 \int \frac{\partial G_0(\alpha,\beta)}{\partial n_\alpha}\frac{\partial G_0(\beta,r')}{\partial n_\beta} dS_\beta \\ &\quad + 2^3 \int \frac{\partial G_0(\alpha,\beta)}{\partial n_\alpha}\frac{\partial G_0(\beta,\gamma)}{\partial n_\beta}\frac{\partial G_0(\gamma,r')}{\partial n_\gamma} dS_\beta dS_\gamma \\ &\quad - \cdots \Bigg]. \end{aligned} \tag{A5}$$

The terms in Eq. (A5) can be looked upon as one-, two-, and three-scattering terms as

$$\Sigma_1 = 2\int d^3r' \frac{\partial G_0(\alpha,r')}{\partial n_\alpha}, \tag{A6}$$

$$\Sigma_2 = -2^2 \int \frac{\partial G_0(\alpha,\beta)}{\partial n_\alpha}\frac{\partial G_0(\beta,r')}{\partial n_\beta} dS_\beta d^3r', \tag{A7}$$

$$\Sigma_3 = 2^3 \int \frac{\partial G_0(\alpha,\beta)}{\partial n_\alpha}\frac{\partial G_0(\beta,\gamma)}{\partial n_\beta}\frac{\partial G_0(\gamma,r')}{\partial n_\gamma} dS_\beta dS_\gamma d^3r'. \tag{A8}$$

Equation (A6) may be expanded through the local surface coordinates α, β, and γ. For a weakly curved surface where the Debye-Hückel screening length is much smaller than the smallest scale of curvature, the scattering kernel $\partial G_0(\beta^+,\alpha)/\partial n_\alpha$ is expressed through a local coordinate system [50,51] with the z axis parallel to an inward normal vector n_α and a tangent plane on which the projection is made. The local equation of surface S in terms of curvature radii $R_1(\alpha)$ and $R_2(\alpha)$,

$$z_\alpha = (1/2)[x^2/R_1(\alpha) + y^2/R_2(\alpha)] + \cdots, \tag{A9}$$

is introduced to Eq. (A6) through the surface area element $dS_\beta = \sqrt{g}dxdy$, where $g = 1 + [\nabla z_\alpha(x,y)]^2$. Using $\partial/\partial n_\alpha \equiv -\partial/\partial z$, the kernel $\partial G_0(\alpha,\beta)/\partial n_\alpha$ under planar approximation [50] reads to first order $\partial G_0(\alpha,\beta)/\partial n_\alpha = -(z/\rho)[\partial G_0(\rho)/\partial\rho]$, where $\rho = |\alpha' - \beta'| = (x^2+y^2)^{1/2}$ is the distance in the tangent plane and $G_0 = \exp(-\rho)/4\pi\rho$ is the Green's function in the tangent plane. Now we can rewrite the one-scattering integral (A6) as

$$\Sigma_1 = 2\int dx\,dy \left[G_0(\rho) + \frac{1}{2}\frac{z^2}{\rho}\frac{\partial G_0}{\partial\rho}\right], \tag{A10}$$

which is further simplified using the angular averages $\langle\cdot\rangle$

$$\begin{aligned} \frac{1}{\rho^2}\langle z_\alpha\rangle &= \frac{1}{2}\int_0^{2\pi} d\theta \left(\frac{\cos^2\theta}{R_1(\alpha)} + \frac{\sin^2\theta}{R_2(\alpha)}\right) \\ &= \frac{\pi}{2}\left(\frac{1}{R_1(\alpha)} + \frac{1}{R_2(\alpha)}\right), \end{aligned} \tag{A11}$$

$$\begin{aligned} \frac{1}{\rho^4}\langle z_\alpha^2\rangle &= \frac{1}{4}\int_0^{2\pi} d\theta \left(\frac{\cos^2\theta}{R_1(\alpha)} + \frac{\sin^2\theta}{R_2(\alpha)}\right)^2 \\ &= \frac{3\pi}{8}\left(\frac{1}{R_1(\alpha)^2} + \frac{1}{R_2(\alpha)^2}\right) + \frac{\pi}{4R_1(\alpha)R_2(\alpha)}. \end{aligned} \tag{A12}$$

Substituting Eq. (A11) into (A10) and integrating over ρ, we finally get the one-scattering term as

$$\Sigma_1 = \frac{1}{\kappa} - \frac{1}{\kappa^3}\left(\frac{3}{2R(\alpha)^2} - \frac{1}{2R_1(\alpha)R_2(\alpha)}\right) + O\left(\frac{1}{R^3}\right), \tag{A13}$$

where $H_\alpha = 1/R(\alpha) = (1/2)[1/R_1(\alpha) + 1/R_2(\alpha)]$ and $K_\alpha = 1/R_1(\alpha)R_2(\alpha)$. Similarly, on iteration in Eqs. (A7) and (A8) two- and three-scattering terms are obtained as

$$\Sigma_2 = -\frac{1}{\kappa^2}\frac{1}{R(\alpha)} + O\left(\frac{1}{R^3}\right), \quad \Sigma_3 = \frac{1}{\kappa^3}\frac{1}{R(\alpha)^2} + O\left(\frac{1}{R^3}\right). \tag{A14}$$

Now substituting Eqs. (A13) and (A14) into Eq. (A5), after simplification the capacitance density at position α is

$$c(H_\alpha, K_\alpha) = \frac{\epsilon\kappa}{4\pi}\left[1 - \frac{1}{\kappa}H_\alpha - \frac{1}{2\kappa^2}(H_\alpha^2 - K_\alpha) + \cdots\right]. \tag{A15}$$

APPENDIX B

The surface capacitance $\langle c_S\rangle$ (F/cm^2) given by Eqs. (20), (22), and (24) can be converted to the volumetric capacitance $\langle c_V\rangle$ (F/cm^3) as

$$\langle c_V\rangle = \langle c_S\rangle\frac{A}{V_0}, \tag{B1}$$

where A denotes the total microscopic area of the electrode and V_0 denotes the macroscopic volume of the electrode. The total microscopic area of nanoporous membrane (forest of nanorods) with a cylindrical pore (rod) is $A = 2\pi r l N_i$ where

$$N_i = \frac{V_i}{\pi r^2 l}, \tag{B2}$$

where V_i is the microscopic volume of the electrode, $\pi r^2 l$ is the volume of a single pore or rod, and N_i is the number of pores ($N_i = N_h$) in the case of a nanoporous membrane electrode and the number of connected rods ($N_i = N_c$) in the case of a nanoforest electrode. The microscopic volume of a nanoporous membrane may be related to the macroscopic volume of an electrode as $V_i = \Phi V_0$, where Φ is the porosity of the material. Similarly, the microscopic volume of a forest of nanopores may be written as $V_i = (1-\Phi)V_0$. Now the volumetric capacitance of a nanoporous membrane electrode may be written using Eq. (B1) as $\langle c_V\rangle = \langle c_S\rangle(2\Phi/r)$. Similarly, the volumetric capacitance of a nanoforest electrode may be written using Eq. (B1) as $\langle c_V\rangle = \langle c_S\rangle[2(1-\Phi)/r]$.

[1] P. Simon and Y. Gogostsi, Nat. Mater. **7**, 845 (2008).
[2] R. H. Baughman, A. A. Zakhidov, and W. A. de Heer, Science **297**, 787 (2002).
[3] R. B. Schoch, J. Han, and P. Renaud, Rev. Mod. Phys. **80**, 839 (2008).
[4] L. L. Zhang and X. S. Zhao, Chem. Soc. Rev. **38**, 2520 (2009).
[5] Y. Gogotsi, A. Nikitini, H. Ye, W. Zhou, J. E. Fischer, B. Yi, H. C. Foley, and M. W. Barsoum, Nat. Mater. **2**, 591 (2003).
[6] T. Ohkubo *et al*., Phys. Scr. **T115**, 685 (2005).
[7] S. K. Rangarajan, in *Electrochemistry: A Specialist Periodical Report*, edited by H. R. Thirsk (The Chemical Society, London 1980), Vol. 7.
[8] B. E. Conway, *Electrochemical Supercapacitor: Scientific Fundamentals and Technological Applications* (Kluwer, Dordrecht, 1999).
[9] M. Z. Bazant, K. Thornton, and A. Ajdari, Phys. Rev. E **70**, 021506 (2004).
[10] M. Z. Bazant, M. S. Kilic, B. D. Storey, and A. Ajdari, Adv. Colloid Interface Sci. **152**, 48 (2009).
[11] P. M. Biesheuvel and M. Z. Bazant, Phys. Rev. E **81**, 031502 (2010).
[12] M. S. Kilic, M. Z. Bazant, and A. Ajdari, Phys. Rev. E **75**, 021502 (2007).
[13] M. Eikerling, A. A. Kornyshev, and E. Lust, J. Electrochem. Soc. **152**(1), E24 (2005).
[14] G. Gryglewicz, J. Machnikowski, E. L. Grabowska, G. Lota, and E. Frackowiak, Electrochim. Acta **50**, 1197 (2005).
[15] J. Chmiola, G. Yushin, Y. Gogotsi, C. Portet, P. Simon, and P. L. Taberna, Science **313**, 1760 (2006).
[16] C. Largeot, C. Portet, J. Chmiola, P. L. Taberna, Y. Gogotsi, and P. Simon, J. Am. Chem. Soc. **130**, 2730 (2008).
[17] J. Huang, B. G. Sumpter, V. Meunier, G. Yushin, C. Portet, and Y. Gogotsi, J. Mater. Res. **25**, 1525 (2010).
[18] J. Huang, B. G. Sumpter, and V. Meunier, Chem. Eur. J **14**, 6614 (2008).
[19] G. Feng, R. Qiao, J. Huang, B. G. Sumpter, and V. Meunier, ACS Nano **4**(4), 2382 (2010).
[20] P. M. Biesheuvel, Y. Fu, and M. Z. Bazant, Phys. Rev. E **83**, 061507 (2011).
[21] P. M. Biesheuvel, Y. Fu, and M. Z. Bazant, Russ. J. Electrochem. **48**, 580 (2012).
[22] P. M. Biesheuvel, R. Zhao, S. Porada, and A. van der Wal, J. Colloid Interface Sci. **360**, 239 (2011).
[23] S. Porada, L. Weinstein, R. Dash, A. van der Wal, M. Bryjak Y. Gogotsi, and P. M. Biesheuvel, ACS Appl. Mater. Interfaces **4**, 1194 (2012).
[24] Raul A. Rica, D. Brogioli, R. Ziano, D. Salerno, and F. Mantegazza, J. Phys. Chem. C **116**, 16934 (2012).
[25] R. Zhao, P. M. Biesheuvel, H. Miedema, H. Bruning, and A. van der Wal, J. Phys. Chem. Lett. **1**, 205 (2010).
[26] R. Zhao, M. van Soestbergen, H. H. M. Rijnaarts, A. van der Wal, M. Z. Bazant, and P. M. Biesheuvel, J. Colloid Interface Sci. **384**, 38 (2012).
[27] T. Nagy, D. Henderson, and D. Boda, J. Phys. Chem. B **115**, 11409 (2011).
[28] G. M. Torrie and J. P. Valleau, J. Chem. Phys. **86**, 3251 (1982).
[29] D. Boda, W. R. Fawcett, D. Henderson, and S. Sokolowski, J. Chem. Phys. **116**, 7170 (2002).
[30] K. Kiyohara, T. Sugino, and K. Asaka, J. Chem. Phys. **132**, 144705 (2010); **134**, 154710 (2011).
[31] L. Yang, B. H. Fishbine, A. Migliori, and L. R. Pratt, J. Am. Chem. Soc. **131**, 12373 (2009).
[32] T. Goel, C. N. Patra, S. K. Ghose, and T. Mukherjee, J. Phys. Chem. B **115**, 10903 (2011).
[33] Y. Shim and H. J. Kim, ACS Nano **4**, 2345 (2010).
[34] A. Tanimura, A. Kovalenko, and F. Hirata, Chem. Phys. Lett. **378**, 638 (2003).
[35] A. Tanimura, A. Kovalenko, and F. Hirata, Langmuir **23**, 1507 (2007).
[36] H. Wang and L. Pilon, J. Phys. Chem. C **115**, 16711 (2011).
[37] H. Wang, J. Vargehese, and L. Pilon, Electrochim. Acta **56**, 6189 (2011).
[38] S. Yoon, S. M. Oh, C. W. Lee, and J. H. Ryu, J. Electroanal. Chem. **650**, 187 (2011).
[39] E. J. F. Dickinson and R. G. Compton, J. Phys. Chem. C **113**, 17585 (2009).
[40] J. Huang, R. Qiao, B. G. Sumpter, and V. Meunier, J. Mater. Res. **25**, 1469 (2010).
[41] H. L. F. von Helmholtz, Ann. Phys. (Leipzig) **243**, 337 (1879).
[42] G. Gouy, J. Phys. Theor. Appl. **9**, 457 (1910).
[43] D. L. Chapman, Philos. Mag. Ser. **6**, 475 (1913).
[44] O. Stern, Z. Elektrochem. **30**, 508 (1924).
[45] B. Duplantier, Electrochim. Acta **36**, 1757 (1991).
[46] O. Pecina and J. P. Badiali, Phys. Rev. E **58**, 6041 (1998).
[47] R. E. Goldstein, A. I. Pesci, and V. Romero-Rochin, Phys. Rev. A **41**, 5504 (1990).
[48] R. Kant and S. K. Rangarajan, J. Electroanal. Chem. **396**, 285 (1995).
[49] F. Tessier and G. W. Slater, Electrophoresis **27**, 686 (2006).
[50] R. Balian and C. Bloch, Ann. Phys. (NY) **60**, 401 (1970); **84**, 559 (1974).
[51] B. Duplantier, R. E. Goldstein, V. Romero-Rochin, and A. I. Pesci, Phys. Rev. Lett. **65**, 508 (1990).
[52] B. Duplantier, Physica A **168**, 179 (1990).
[53] R. Kant, Ph.D. thesis, Indian Institute of Science, 1993.
[54] R. Kant and S. K. Rangarajan, J. Electroanal. Chem. **552**, 141 (2003).
[55] R. Kant, J. Phys. Chem. B **101**, 3781 (1997).
[56] R. Kant and S. K. Rangarajan, J. Electroanal. Chem. **368**, 1 (1994).
[57] R. Kant, Phys. Rev. Lett. **70**, 4094 (1993).
[58] L. I. Daikhin, A. A. Kornyshev, and M. Urbakh, J. Chem. Phys. **108**, 1715 (1998).
[59] C. H. Arns, M. A. Knackstedt, and K. R. Mecke, Colloids Surf. A **241**, 351 (2004).
[60] M. C. Henstridge, E. J. F. Dickinson, and R. G. Compton, Chem. Phys. Lett. **485**, 167 (2010).
[61] H. Gerischer, J. Phys. Chem. **89**, 4249 (1985).
[62] H. Gerischer, R. McIntyre, D. Scherson, and W. Storck, J. Phys. Chem. **91**, 1930 (1987).
[63] M. P. do Carmo, *Differential Geometry of Curves and Surfaces* (Prentice-Hall, Englewood Cliffs, NJ, 1976).
[64] L. I. Daikhin, A. A. Kornyshev, and M. Urbakh, Phys. Rev. E **53**, 6192 (1996).
[65] E. Lust, A. Jänes, T. Pärn, and P. Nigu, J. Solid State Electrochem. **8**, 224 (2004).
[66] D. W. Wang, F. Li, M. Lui, G. Q. Lu, and H. M. Cheng, Angew. Chem. Int. Ed. **47**, 373 (2008).
[67] R. J. Adler, *The Geometry of Random Fields* (Wiley, New York, 1981).

[68] K. R. Mecke, Int. J. Mod Phys. B **12**, 861 (1998).
[69] J. M. Elliott and J. R. Owen, Phys. Chem. Chem. Phys. **2**, 5653 (2000).
[70] R. Kant and S. K. Rangarajan, J. Electroanal. Chem. **277**, 19 (1990).
[71] O. Barbieri, M. Hahn, A. Herzog, and R. Kötz, Carbon **43**, 1303 (2005).
[72] M. B. Singh and R. Kant, Proc. R. Soc. A **469**, 20130163 (2013).
[73] P. L. Taberna, S. Mitra, P. Poizot, P. Simon, and J. M. Tarascon, Nat. Mater. **5**, 567 (2006).
[74] J. Benson, S. Boukhalfa, A. Magasinski, A. Kvit, and G. Yushin, ACS Nano **6**, 118 (2012).
[75] C. J. E. Farina and K. B. Oldham, J. Electroanal. Chem. **81**, 21 (1977).
[76] C. H. Hou, C. Liang, S. Yiacoumi, S. Dai, and C. Tsouris, J. Colloid Interface Sci. **302**, 54 (2006).
[77] M. Ue, J. Electrochem. Soc. **141**, 3336 (1994).
[78] J. Chmiola, C. Largeot, P. L. Taberna, P. Simon, and Y. Gogotsi, Angew. Chem. Int. Ed. **47**, 3392 (2008).
[79] S. Kondrat and A. A. Kornyshev, J. Phys. Condens. Matter **23**, 022201 (2011).
[80] S. Kondrat, N. Georgi, M. V. Fedorov, and A. A. Kornyshev, Phys. Chem. Chem. Phys. **13**, 11359 (2011).
[81] C. Merlet, B. Rotenberg, P. A. Madden, P.-L. Taberna, P. Simon, Y. Gogotsi, and M. Salanne, Nat. Mater. **11**, 306 (2012).
[82] D. Jiang, Z. Jin, D. Henderson, and J. Wu, J. Phys. Chem. Lett. **3**, 1727 (2012).
[83] D. Jiang, Z. Jin, and J. Wu, Nano Lett. **11**, 5373 (2011).
[84] G. Feng and P. T. Cummings, J. Phys. Chem. Lett. **2**, 2859 (2011).
[85] D. Henderson, J. Colloid Interface Sci. **374**, 345 (2012).
[86] K. B. Oldham, J. Electroanal. Chem. **613**, 131 (2008).
[87] O. K. Rice, Phys. Rev. **31**, 1051 (1928).
[88] A. A. Kornyshev, W. Schmickler, and M. A. Vorotyntsev, Phys. Rev. B **25**, 5244 (1982).
[89] B. Skinner, T. Chen, M. S. Loth, and B. I. Shklovskii, Phys. Rev. E **83**, 056102 (2011).